Receptor-mediated adhesion phenomena

Model studies with the Radial-Flow Detachment Assay

Cindi Cozens-Roberts, John A. Quinn, and Douglas A. Lauffenburger
Department of Chemical Engineering, University of Pennsylvania, Philadelphia, Pennsylvania 19104 USA

ABSTRACT Receptor-mediated cell adhesion phenomena play a vital role in many physiological and biotechnology-related processes. To investigate the physical and chemical factors that influence the cell/surface interaction, we have used a radial flow device, a so-called Radial-Flow Detachment Assay (RFDA). The RFDA allows us to make direct observations of the detachment process under specified experimental conditions. In results reported here, we have studied the detachment of receptor-coated latex beads (prototype cells) from ligand-coated glass surfaces. The receptors and ligands used in this work are complementary antibodies. The beads enable us to examine several aspects of the adhesion process with particles having uniform properties that can be varied systematically. Advantages of the RFDA are many, especially direct observation of cell detachment over a range of shear stresses with quantitative measurement of the adhesive force. We focus our studies on the effects of ligand and receptor densities, along with the influence of pH and ionic strength of the medium. These data are analyzed with a mathematical model based on the theoretical framework of Bell, G. I. (1978. *Science [Wash. DC]*. 200:618–627) and Hammer, D. A. and D. A. Lauffenburger (1987. *Biophys. J.* 52:475–487). We demonstrate experimental validation of a theoretical expression for the critical shear stress for particle detachment, and show that it is consistent with reasonable estimates for the receptor-ligand bond affinity.

INTRODUCTION

Receptor-mediated cell adhesion to surfaces, including other cells as well as biomaterials, is an important element of many physiological and biotechnology-related processes. For example, when tissue becomes infected neutrophils migrate from the bloodstream into the tissue by first adhering to the endothelial cells that line the blood vessel walls through an interaction that is thought to be modulated by receptor and/or ligand expression (3). Also, the homing of lymphocytes to Peyer's patches and lymph nodes is mediated by receptor interactions with organ-specific molecules on the surface of the high endothelial cells that line the venules (4, 5). Biotechnological examples that may involve receptor-mediated adhesion include cell/biomaterial interactions (6, 7) and cell separation techniques, such as cell affinity chromatography (CAC) (8, 9). In CAC, ligand that binds to specific receptors on the target cell population is coupled to a surface (generally beads or membranes) over which the cell mixture of interest is passed. The target cells bind preferentially and the unbound cells are rinsed away. CAC has been used to purge bone marrow contaminated with 1% tumor cells to 0.0001% (8).

Address correspondence to Dr. John A. Quinn, Department of Chemical Engineering, University of Pennsylvania, 220 South 33rd Street, Philadelphia, PA 19104.

The adhesive interaction between a cell and a surface, which may involve both nonspecific interactions (such as van der Waals, electrostatic, and steric stabilization) and specific receptor-ligand bonds, depends on the cell and surface properties, the medium composition, and the external forces, such as depositional and hydrodynamic forces. Due to the complexity of this interaction, in vitro methods have been developed to study cell-to-surface adhesion. Detachment assays are used to compare the ability of adherent cells to withstand a given force. An excellent review on the various detachment assays can be found in Hubbe (10). In general, the major difference between the assays is the method used to exert force on the cells. Typically, the methods fall into one of three categories: micromanipulation, centrifugation, or hydrodynamic shear. In micromanipulation, the cell is held in a micropipette and brought into contact with an affinity surface. After a specified amount of time, the cell is withdrawn from the receiving surface with the micropipette by increasing suction pressure. This assay has been used to generate useful information on the adhesive force between a cell and a surface and on the mechanical properties of the cell membrane (11–13). In centrifugation, cells are allowed to settle onto the surface under the influence of gravity, and, after a given amount of time, are centrifuged. The ratio of the number of adherent cells after centrifugation to the number before provides an

0006-3495/90/07/107/19 $2.00

TABLE 1 Estimated parameter values

Parameter	Symbol	Range for cells	Range for beads
Receptor density	N_R	10^8–10^{13} cm^{-2} (62)	10^{10}–10^{12} cm^{-2}
Ligand density	N_L	10^{10}–10^{12} cm^{-2} (61)	10^{10}–10^{12} cm^{-2}
Contact area radius	a	0.06–1 μm (2)	0.1–0.5 μm
Length of particle to surface bridges	h_s, H	100–300 Å (62)	100–400 Å
Affinity constant	$K°$	10^{-11}–10^{-5} cm^2 (62)	10^{-11}–10^{-8} cm^2
Shear stress	S	0–100 dyn/cm^2 (44)	0–40 dyn/cm^2
Bond number	C	1,000–3,000 (28)	1,000–6,000
Particle radius	ρ_B	3.5–7.5 μm (Leukocyte [79])	4.6–5.1 μm
Specific gravity	—	1.024 (76)	1.05
Particle concentration	c	10^7/ml (CAC [9]) 10^6/ml (Detachment assay [3])	$10^6/ml$

indication of the adhesive force (14, 15). In general, hydrodynamic shear assays can be divided into four categories: flow between parallel plates (16, 17, 18), flow between a rotating and a stationary disc (19, 20), flow between a stationary disc and a rotating cone (similar to a cone-and-plate viscometer) (21), and axisymmetric flow between parallel discs (22–25). The hydrodynamic shear assays can be distinguished by two significant features. First, the parallel plate and rotating cone assays produce only one surface shear stress value per experiment, whereas the rotating disc and axisymmetric assays produce a continuous range of shear stress values within a given experiment. Second, the parallel plate assays are designed for direct observation during shear, whereas the axisymmetric, rotating disc, and rotating cone assays are usually not designed for direct observation. In all three assays, the percentage of cells that remain attached after exposure to a given shear stress provides an indication of the adhesive force.

In vitro detachment studies have enhanced our understanding of the factors involved in cell adhesion. However, the complexity of the interaction and the difficulties associated with measuring key parameters have left many fundamental questions unanswered. Our objective is to combine theoretical models with well-defined experiments to single out the role of certain key parameters on receptor-mediated adhesion. We have begun by developing a simple model cell system to characterize and measure quantitatively important aspects of the adhesive process. Our model system employs 10 μm diam receptor-coated latex beads, using a Radial-Flow Detachment Assay (RFDA) with a ligand-coated glass surface. The beads enable us to examine certain basic aspects of adhesion with particles possessing uniform properties, such as size, shape, and receptor concentration, that can be varied in the range typical for receptor-mediated cell adhesion (Table 1). The RFDA produces an axisymmetric flow field, providing a continuous range of shear stresses within a given experiment. The assay yields a critical radius for adhesion from which the adhesive force can be simply determined. A large shear stress range is available and direct observations can be made under both equilibrium and transient conditions, providing both equilibrium detachment data (reported here) as well as time-dependent attachment and detachment data (26, 27).

The theoretical framework of Bell (1) and of Hammer and Lauffenburger (2) for receptor-mediated cell adhesion is used here to analyze our data on particle adhesion in the RFDA. This framework yields a simple expression for the critical shear stress for detachment as a function of key system parameters. This expression provides a useful basis for the analysis of parameter effects on the adhesive force. In this work, we demonstrate experimental validation of this theoretical expression and further show that it is consistent with reasonable estimates of receptor-ligand bond affinity.

GLOSSARY

- a contact area radius (μm)
- A_v Avogadro's number (mol^{-1})
- c bead concentration (ml^{-1})
- C number of bonds
- d center-to-center bead separation distance (μm)
- F force (dyn)
- h gap width between discs (mm)
- h_s separation distance between bead and plate (μm or Å)
- H maximum distance for receptor-ligand binding (μm or Å)
- k_b Boltzman constant (J/molecule-°K)
- k_f^o forward rate constant (cm^2/min)
- k_r^o reverse rate constant (min^{-1})
- $K°$ affinity constant (cm^2)
- L ligand coating concentration (μg/ml)
- M_w molecular weight
- n number
- N surface density (cm^{-2})
- P probability

Q volumetric flow rate (ml/s)
r radial distance from stagnation point (mm)
R correlation coefficient
Re local Reynolds number
R_T total receptor number per bead
S shear stress (dyn/cm^2)
t time (min)
T temperature (°K)

Subscripts

A active
Ab antibody
b bond
B bead
c critical
E epitope
G glass plate
Gt goat IgG
I inlet
L ligand
P Plexiglass cylinder
R receptor
Rb rabbit anti-goat IgG
s shear
S complementary
T total

Greek characters

β $(K°/33e)(k_bT/\gamma)(a/\rho_B)^3$
γ range of the bond interaction (cm)
λ S_c for net nonspecific force (dyn/cm^2)
μ viscosity (g/cm-s)
ν kinematic viscosity (cm^2/s)
ρ radius (μm or mm)
τ torque (dyn-cm)
ζ no. of adherent beads after shear divided by no. before shear

MATERIALS AND METHODS

Radial-Flow Detachment Assay (RFDA)

The RFDA is shown in Fig. 1. The apparatus consists of two discs, a 50 mm diam optical flat glass plate and a 25.4 mm diam Plexiglass cylinder, separated by a 0.254-mm gap width. The gap width (h) is maintained with three spacers positioned concentically in the region between the Plexiglass cylinder and the side wall. This region, which serves as a reservoir for fluid before exiting through one of three outlets, was included to dampen potential flow disturbances resulting from the spacers, the side wall, and the outlets. The chamber is placed on a stage, a stereo microscope is used to view adhesion to the glass surface, and a constant head tank is used to maintain a given volumetric flow rate (Q) to the chamber. The maximum volumetric flow rate is limited by the criterion that the flow in the inlet pipe be laminar, i.e., the inlet pipe

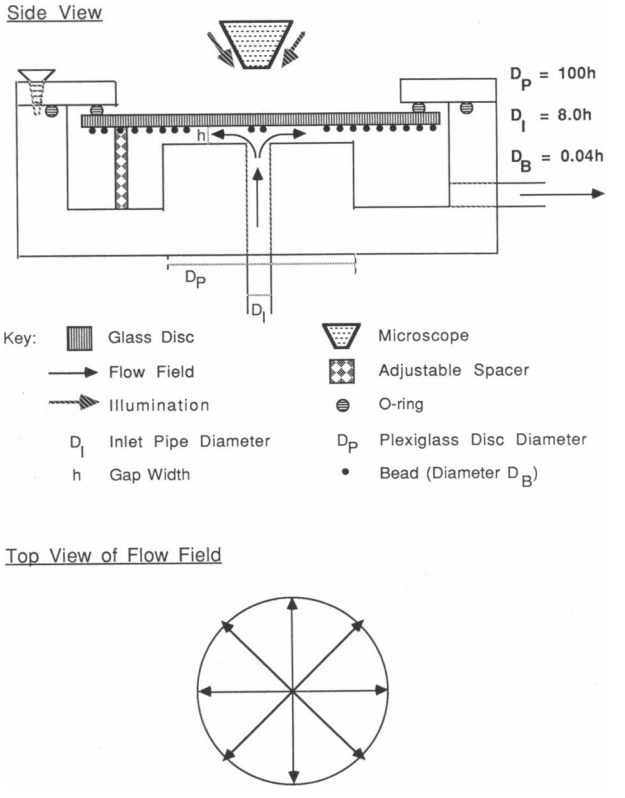

FIGURE 1 Schematic diagram of the Radial-Flow Detachment Assay (RFDA) and the flow field.

Reynolds number be <2,000. In our system, this means $Q \leq 2.7$ ml/s. This criterion also insures local Reynolds numbers (see Eq. 2) <2,000 for chamber radii >0.05 mm, so that an axisymmetric laminar flow field is created between the discs (22, 23). Because the cross-sectional area for flow between the two discs increases radially, the surface stress decreases radially with distance from the central stagnation point. Thus, within a circular zone around the inlet where shear forces are higher (excluding the stagnation point), particles are swept away; however, within the outer zone where shear forces are lower, particles are able to adhere (Fig. 2). The radius that marks the boundary between these two zones defines the critical radius (r_c), the equilibrium position where the force exerted by the fluid on the particle is exactly balanced by the particle-surface adhesive force. In general, r_c is fairly distinct at low magnifications; however, at higher magnifications, this fairly distinct zone is observed to be graduated with respect to the fraction of adherent beads (ζ), where ζ is the number of adherent beads at some time ($t \geq 0$) divided by the number of adherent beads before the initiation of flow (at $t = 0$). As a result, it is difficult to assign a particular value to r_c at these high magnifications; hence, by convention, we define r_c to be the radius where ζ is equal to 0.5 (28–31).

Receptors and ligand

In the present experiments, goat IgG and rabbit anti-goat IgG were used to simulate the ligand/receptor interaction. Rabbit anti-goat IgG is a polyclonal antibody from rabbit that binds to goat IgG (Appendix 1).

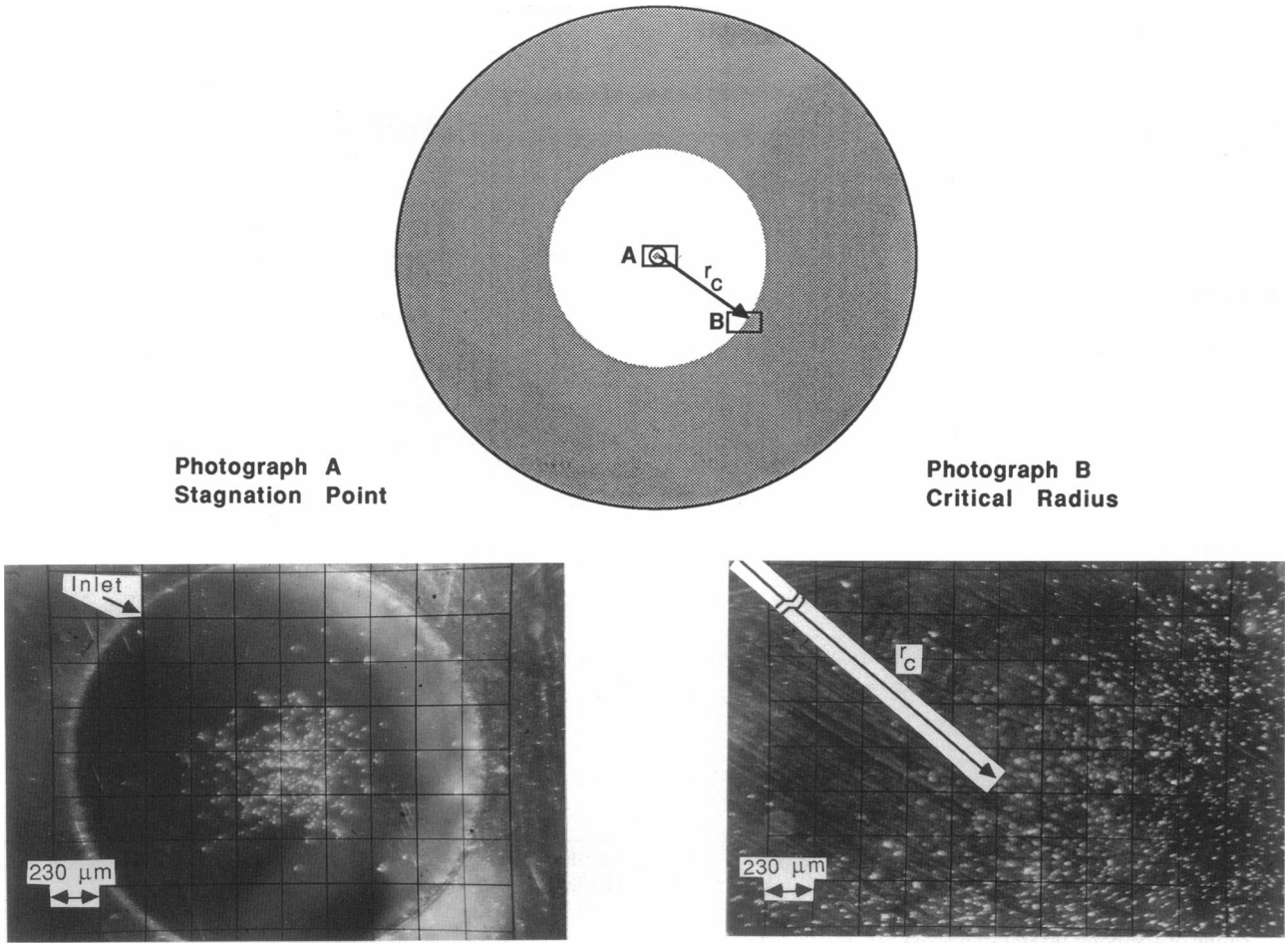

FIGURE 2 Schematic diagram of the pattern for adhesion with photographs of the regions encompassing the stagnation point and the critical radius.

Both antibodies were purchased from Sigma Immuno Chemicals (St. Louis, MO) as affinity purified immunoglobulin and were used without additional purification.

Plate preparation

Optically flat glass discs (50 mm diam, 3 mm thick) were cleaned and then treated with 3-aminopropyltriethoxysilane in acetone. This procedure covalently couples 3-aminopropyltriethoxysilane to the glass surface, forming an alkylamine carrier (32). The uniformity of the coating was checked by testing the hydrophobicity of the disc surface. The criterion for an even coating is when a 20-μl drop of treated water placed on the disc surface can move freely and continuously when the tilt angle of the disc is >40 degrees (33). The water used to test the hydrophobicity of the plates and to make up the protein and flow cell feed solutions was passed through two deionizers, a carbon tank (to remove dissolved organic contaminants), and a 0.22-μm filter (to exclude bacteria). In general, the pH of the treated water was 7.6. After silanization, ligand (for example, goat IgG or rabbit anti-goat IgG) was coupled to the disc by means of glutaraldehyde chemistry, which covalently binds the ligand via an amine group to an aldehyde group on the glass plate. Incubation steps were carried out in a Petri dish, wash steps were performed by placing the disc in a large Petri dish of treated water, and all liquid surfaces were aspirated before the disc was pulled through the air/liquid interface to remove surface contaminates. Glycine was used to deactivate any remaining aldehyde groups on the glass surface. The incubation times with glutaraldehyde, ligand, and glycine were 30 min, 2 h, and 1 h, respectively. Ligand-coated discs were stored at 4–6°C in storage buffer (PBS pH 7.4 with sodium azide [NaN_3] as a preservative and bovine serum albumin [BSA]) and were used within 1–2 d.

Latex microsphere preparation

10 μm diam carboxylated latex microspheres were purchased from Polysciences, Inc. (Warrington, PA). The beads are produced by a linear polymerization of polystyrene, whose characteristic hydrophobic interactions contribute to their resistance to both elastic and plastic deformation, i.e., they do not deform on contact with a surface (D. Fannon, Polysciences, Inc., personal communication). The beads were coated with receptors (for example, goat IgG or rabbit anti-goat IgG) by means of carbodiimide chemistry, which covalently binds the receptor via an amine group to an activated carboxylate group on the sphere (34). Wash steps were done with a glass frit (size 4–8 μm) and incubation steps in a 1.5-ml capacity centrifuge tube placed on a rocker to insure uniform mixing. Ethanolamine was used to block unreacted sites on the beads and BSA to block nonspecific binding sites. The incubation times

with carbodiimide, receptor, ethanolamine, and BSA were 2 h, 4 h, 1 h, and 30 min, respectively. The beads were stored at 4–6°C in storage buffer, which also contained glycerol, and used within one month of coating. The concentration of the bead solutions was determined by measuring the absorbance at 292 nm, and determining the corresponding concentration from a standard curve of absorbance vs. concentration.

Coating density

The total receptor density per bead was determined from a material balance. This analysis requires values for the receptor concentrations of the incubation and the wash solutions and the number of beads coated. The BCA assay (Pierce Chemical Co., Rockford, IL) was used to determine the protein concentration of the wash. A protein assay such as BCA or Coomassie Blue was not used to determine the total ligand density on a plate because the concentration in the wash was too small for the assay to be reliable; therefore, this density is estimated (Appendix 1). Amine coupling of IgG to a surface is known to result in a loss of binding capacity (35, 36); therefore, several assumptions are used to estimate values for the effective receptor and ligand densities (Appendix 1). It is important to realize that the assumptions made in Appendix 1 affect the quantitative values but not the qualitative behavior of these data because the relative coating densities (coating density ratios) are not affected by the assumptions. In other words, the assumptions provide absolute (effective) values for the coating densities, and, even if they are not precisely correct, the trends for these data will not change. In addition, the specific binding capacity of 0.063 that we estimate for immobilized rabbit anti-goat IgG is in excellent agreement with the measured value of 0.06 obtained by Cress and Ngo (37) for the specific binding capacity of rabbit anti-human IgG immobilized to a surface via its amine groups.

Procedure for equilibrium detachment experiments

To start an experiment, the bottom portion of the RFDA is filled with fluid and the coated glass plate is placed on the spacers. The chamber is assembled insuring constant torque is applied to the screws that hold the flow cell together to prevent bending or distortion of the glass disc. Unless otherwise stated, 0.01 M potassium chloride (KCl) was used both to fill the chamber and for the feed. The 0.01 M KCl solutions were prepared with treated water and had a pH of 6.6. After assembling the chamber, the flow cell was inverted and 0.3 ml of receptor-coated bead solution (beads in storage buffer) was slowly injected into the flow cell through a three-way valve in the inlet line. The concentration of the bead solutions was $\sim 8 \times 10^5$ beads/ml, resulting in bead separation distances between 5 and 9 bead diameters. This distance, which is predicted to be 7 bead diameters at this bead concentration (Appendix 2), was chosen to minimize artifacts caused by interactions between particles, such as shielding of the shear field.

The beads were incubated with the coated surface for 30 min. The chamber was placed on the stage, requiring inversion of the chamber with attendant fluid motion. For surfaces coated with the complementary ligand, the small shear stress placed on the particles by this motion is insufficient to detach the beads. The beads were exposed to a constant volumetric flow rate until a stable critical radius developed. In general, this took between 20 and 30 min. The critical radius was measured from the average of four different readings of the stage x-y displacement from the central stagnation point to the critical radius (two Δx readings and two Δy readings). Pictures were taken with a 35-mm camera to provide data for the fraction of adherent beads (ζ) as a function of radial position. The volumetric flow rate was increased in steps and new measurements taken until the critical radius approached 10.5 mm. In general, this procedure gave between two and four data points per plate. The volumetric flow rate vs. critical radius data have an average y-intercept of 2.2 mm, an artifact caused by the inlet effect (22). It is customary to subtract the value for the y-intercept from the data for the critical radius to correct for the entry effect (22, 25); consequently, our results are corrected in this manner. In addition, data are only taken for radii between 2.5 and 10.5 mm to avoid artifacts that may be caused by inlet or outlet effects, respectively. In general, experiments for each ligand coating concentration with each receptor coating concentration were run in duplicate to quadruplicate.

Procedure for ionic strength and pH experiments

The procedure for these experiments was similar to that for the equilibrium detachment experiments with the following exceptions: before assembly the chamber was filled with either treated water or the feed used for the given experiment; sodium chloride (NaCl) solutions were used for feed in the ionic strength studies; sodium hydroxide (NaOH) or hydrogen chloride (HCl) solutions were used for feed in the pH studies; only one flow rate per experiment was examined to maintain a consistent procedure for all of the conditions studied (at harsh conditions, experiments were limited to one data point per plate to reduce the chance of potential artifacts that may be caused by the effect of the medium on the activity of the protein itself); and the critical radius was measured after a 30-min exposure to shear. The NaCl, NaOH, and HCl solutions were made up in treated water (deionized, pH 7.6). Plates coated with 12.5-μg/ml of goat IgG and two types of beads with different rabbit anti-goat IgG receptor densities were used in the present experiments. In general, experiments for each bead type under each condition were run in duplicate or triplicate.

MATHEMATICAL MODEL

In this section, we present the expressions that are used for interpreting our equilibrium detachment data. First, we discuss the parameters that characterize the laminar axisymmetric flow field in the RFDA, in particular, the critical shear stress (S_c). Next, we use the theoretical framework of Bell (1) and of Hammer and Lauffenburger (2) to develop expressions for the total force exerted by the flowing fluid on an adherent particle and the number of bonds required for adhesion at the critical radius. In addition, we develop a simple expression for S_c as a function of certain key parameters, such as the receptor-ligand affinity and the receptor and ligand densities. We then modify this expression to account for the role of a net attractive nonspecific adhesive force.

The conservation of mass and momentum applied to laminar axisymmetric flow provides expressions for the local Reynolds number (Re), surface shear stress (S), and local linear velocity (u) in the RFDA. These three quantities are inversely proportional to radial distance from the central stagnation point (r). For example, the expressions for S and Re are

$$S = 3Q\mu/\pi r h^2 \tag{1}$$

and

$$Re = 2hu_m/\nu = Q/\pi r\nu, \quad (2)$$

respectively, where Q is the volumetric flow rate, μ is the viscosity, h is the gap width between the two discs, ν is the kinematic viscosity, and u_m is the mean velocity. By convention, the hydraulic diameter (2 times h) is the length dimension used in the expression for Re (22, 38). The critical shear stress (S_c), the shear stress at which 50% of the particles remain attached, is determined by using the corrected value for the critical radius (r_c) in Eq. 1.

For a particle to adhere to the surface, the net adhesive force must balance the force and torque imposed by the passing fluid (Fig. 3). The force and torque exerted on an adherent particle in the RFDA are estimated with the expressions of Goldman et al. (39) for a stationary sphere in a shear field. Their expressions predict that both the force and torque are linearly proportional to the surface shear stress (S). The total force exerted by the fluid on an adherent particle is estimated with the force and torque balance developed by Hammer and Lauffenburger (2) for receptor-mediated cell adhesion. Their model is based on the following assumptions: the adhesive force acts both parallel to the direction of flow and normal to the surface of the particle, the nonspecific forces play a negligible role in countering the shear force and torque, and the force per bond and bond density are constant over the contact area. The result for the total fluid force exerted on an adherent particle at the critical radius is:

$$F_T \approx 110 S_c \rho_B^3/a, \quad (3)$$

where ρ_B and a are the radius of the bead and contact area, respectively (Appendix 3).

The rate of bond formation is governed by the following kinetic equation:

$$(dN_b/dt) = k_f^\circ(N_L - N_b)(N_R - N_b) - k_r^\circ N_b, \quad (4)$$

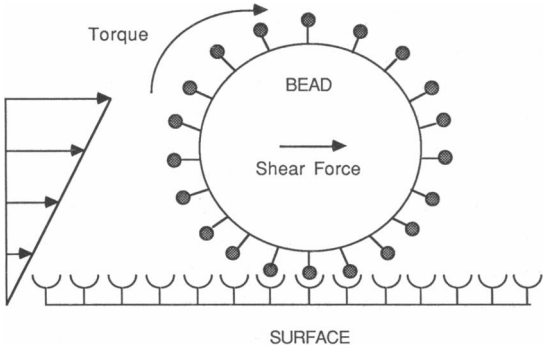

FIGURE 3 Illustration of the force and torque imposed by the passing fluid.

where N_b, N_L, and N_R are the bond, ligand, and receptor surface densities, respectively, and k_f° and k_r° are the forward and reverse rate constants, respectively. The hydrodynamic force exerted on an adherent cell stresses the bonds, decreasing the duration of each interaction as well as the equilibrium bond density. Bell (1) models the effect of an external force on the bonds by replacing the reverse rate constant by k_r, where:

$$k_r = k_r^\circ \exp(\gamma F_T/Ck_bT), \quad (5)$$

where C is the total number of receptor-ligand complexes ($C = \pi a^2 N_b$), k_b is the Boltzman constant, T is the temperature, and γ is the range of the interaction ($\sim 5 \times 10^{-8}$ cm for an antigen-antibody bond [1]). This expression, which is adapted from work by Zhurkov (40) on the kinetic theory of the strength of solids, is based on the following assumptions: the bond density is uniform, the bonds are equally stressed, and the contribution from the nonspecific forces to the adhesive force is negligible. These same assumptions are used with the expression developed by Bell (1) for the force of a bond to estimate the number of bonds required for adhesion at the critical radius:

$$C \approx (160\gamma/k_bT)(S_c/\ln(K^\circ N_L))(\rho_B^3/a), \quad (6)$$

where K° is the receptor-ligand affinity constant (k_f°/k_r°) (Appendix 3). This equation predicts that the number of bonds required for adhesion at a given critical shear stress is directly proportional to that shear stress. The total receptor density required for adhesion is estimated with the expression developed by Hammer and Lauffenburger (2) for equilibrium adhesion. The result for the RFDA is rearranged to (Appendix 3):

$$S_c \approx \beta N_L N_R, \quad (7)$$

where:

$$\beta = (K^\circ/33e)(k_bT/\gamma)(a/\rho_B)^3.$$

This expression predicts that S_c is linearly proportional to the receptor density, the ligand density, and the parameter β, where β is linearly proportional to the receptor-ligand affinity and to the cube of the contact area radius divided by the particle radius. Eq. 7 is applicable to receptor-mediated adhesion with a negligible contribution from the nonspecific forces to the adhesive force. For certain particle-to-surface interactions, however, nonspecific forces do play a role in countering the hydrodynamic force. We account for the effect of a net attractive nonspecific adhesive force by modifying Eq. 7 as follows:

$$S_c \approx \beta N_L N_R + \lambda, \quad (8)$$

where λ is the critical shear stress that would be measured in the absence of specific forces. In the present experiments, β is assumed to be a constant for a given medium; therefore, we predict that a plot of N_R or of N_L vs. S_c is linear with a y-intercept of λ and a slope of βN_L or βN_R, respectively. This is an important test of this theoretical framework, along with examination of the value of β in light of reasonable system parameter estimates.

RESULTS

This section contains our results for the detachment of receptor-coated beads (prototype cells) from ligand-coated surfaces under specified experimental conditions. First, we present data to show the reliability and reproducibility of the RFDA. Next, we present results for the effect of various parameters, including intrinsic (receptor and/or ligand-related) and extrinsic (medium-related) factors, on the adhesive force.

Proof of assay

Axisymmetric flow field

The adhesion pattern that forms on exposure to shear is used to verify the symmetry of the radial flow field. The pattern consists of beads attached at and about the stagnation point and at and beyond the critical radius (Fig. 2).

Specific and nonspecific binding

In general, the adhesive force between a particle and surface is stronger with receptor-ligand bonds (specific adhesion) than without (nonspecific adhesion) (20, 41), therefore, specific binding was verified by performing equilibrium detachment experiments with goat IgG coated beads and discs coated with either rabbit anti-goat IgG, glycine, or rabbit IgG (Fig. 4). These disc coatings were chosen because rabbit anti-goat IgG is the complementary ligand, glycine is used to deactivate remaining aldehyde groups on the ligand-coated surface (Materials and Methods), and rabbit IgG provides a measure of the net contribution of nonspecific forces to the bond between rabbit anti-goat IgG and goat IgG (42, 43). The data presented in Fig. 4*b* show that the adhesive force is greatest between the goat IgG coated beads and rabbit anti-goat IgG coated surfaces, which is consistent with specific binding, and that the adhesive interaction with the glycine coated surface, whereas not as strong as that with the specific surface, is stronger than that with the rabbit IgG coated surface. The small nonspecific adhesive force between the goat IgG coated beads and the rabbit IgG coated surfaces can be interpreted as a small contribution from nonspecific forces to the net strength of the rabbit anti-goat IgG/goat IgG interaction. In addition, we examined the nonspecific interaction between rabbit antigoat IgG coated beads and glycine coated surfaces. Here, the nonspecific adhesive force is weak, with ~70% detachment on inversion of the chamber to place it on the stage ($S - S_o = 0$ dyn/cm^2).

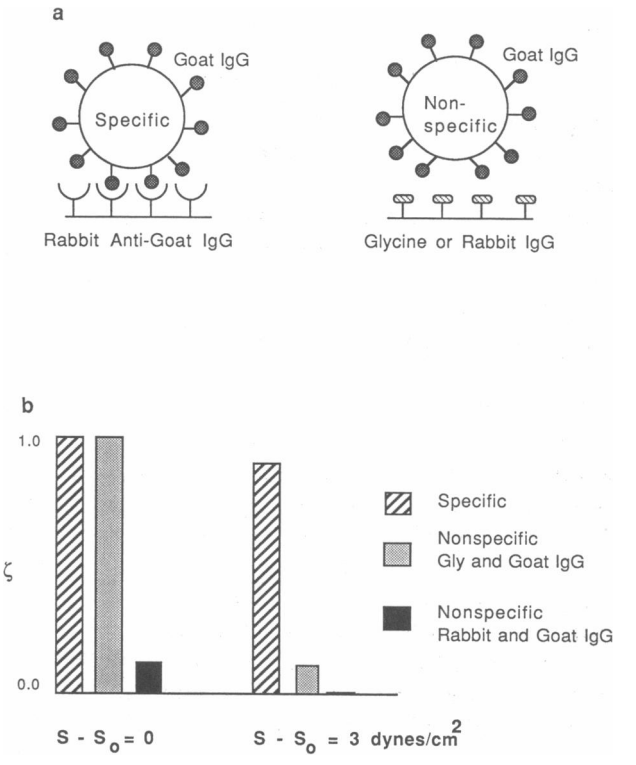

FIGURE 4 (*a*) Schematic diagram of specific and nonspecific binding between goat IgG receptors on the bead surface and rabbit anti-goat IgG and glycine or rabbit IgG on the plate, respectively. (*b*) The number of adherent goat IgG coated beads after exposure to shear divided by the number before shear (ζ) for plates coated with either rabbit anti-goat IgG, glycine, or rabbit IgG. S_o is the small shear stress caused by attendant fluid motion on inverting the flow cell to place it on the stage.

Reproducibility

For laminar axisymmetric flow, the critical shear stress (S_c) is directly proportional to the volumetric flow rate (Q) divided by the critical radius (r_c) (Eq. 1). S_c should remain constant for experiments run under identical conditions; consequently, the slope of the Q vs. r_c data should also remain constant. Therefore, reproducibility is demonstrated by plotting on the same graph Q vs. r_c data obtained for experiments run under identical conditions and determining the resulting correlation coefficient (R). An example of the reproducibility of the data is seen in Fig. 5. Fig. 5 is a plot of the data obtained for four plates

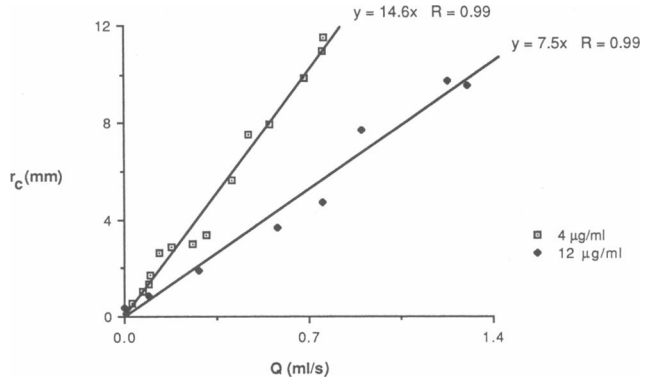

FIGURE 5 Volumetric flow rate (Q) vs. critical radius (r_c) data obtained for four plates each coated with a 4-μg/ml solution and four plates each coated with a 12-μg/ml solution of rabbit anti-goat IgG. Beads with the same goat IgG receptor density were used in all eight experiments.

coated with a 4-μg/ml solution of rabbit anti-goat IgG and four plates coated with a 12-μg/ml solution of rabbit anti-goat IgG. Beads with the same total goat IgG receptor number were used in all eight experiments. The correlation coefficients for typical data are between 0.97 and 1.00, with an average value of 0.99.

Intrinsic properties

Ligand concentration

Fig. 6 shows data for the effect of the ligand (rabbit anti-goat IgG) coating concentration (L) on S_c for three bead types (CE, CG, and CD, with ~9.0×10^6, 7.5×10^6, and 5.3×10^6 total goat IgG/bead, respectively). These data indicate that, for a given receptor number, S_c increases linearly as L is increased. In addition, the slope (the increase in S_c with L) increases as R_T increases. The nonzero y-intercept is consistent with the observation that there is a net attractive nonspecific force between goat IgG coated beads and a glycine coated plate (a glycine coated surface is equivalent to coating with a 0-μg/ml ligand solution).

Receptor concentration

The data from Fig. 6 are replotted in Fig. 7 to show that, for a given L, S_c increases linearly with the total goat IgG receptor number (R_T); and that the slope increases as L increases. The nonzero y-intercept in Fig. 7 represents the nonspecific adhesive force between ethanolamine coated beads and a rabbit anti-goat IgG coated surface.

Receptor/ligand interchange

The receptor/ligand interchange consists of reversing the coatings, i.e., coupling rabbit anti-goat IgG to the beads and goat IgG to the plates. Data were obtained with three bead types: Cl with ~7.2×10^6, and CJ and CL, each with ~3.6×10^6 total rabbit anti-goat IgG/bead. The reproducibility of the Q vs. r_c data obtained with this configuration is identical to that for the reverse configuration, having an average correlation coefficient of 0.99. Fig. 8 shows the effect of varying the total rabbit anti-goat IgG receptor number as well as the goat IgG ligand coating concentration. The trends for these data are similar to those for the data in Fig. 7. The y-intercept is, however, significantly lower, consistent with the nonspecific data on the interaction between rabbit IgG and goat IgG coated surfaces (a rabbit IgG coated surface is equivalent to a receptor number of zero because, for these experiments, receptor number was varied with rabbit IgG [the ratio of rabbit anti-goat IgG to rabbit IgG on a bead is assumed to be equal to the ratio in the incubation solution]).

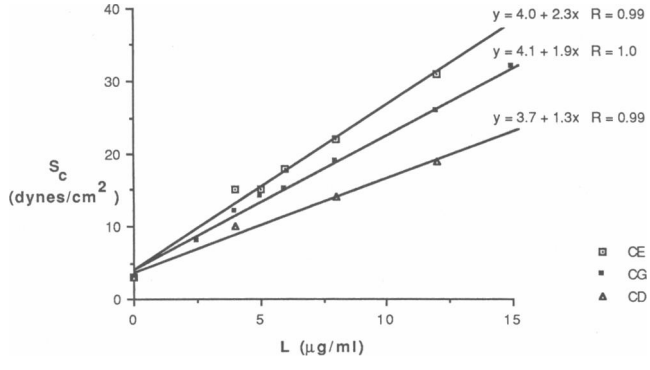

FIGURE 6 Ligand (rabbit anti-goat IgG) coating concentration (L) vs. critical shear stress (S_c) data for three bead types: CE, CG, and CD with ~9.0×10^6, 7.5×10^6, and 5.3×10^6 total goat IgG/bead, respectively.

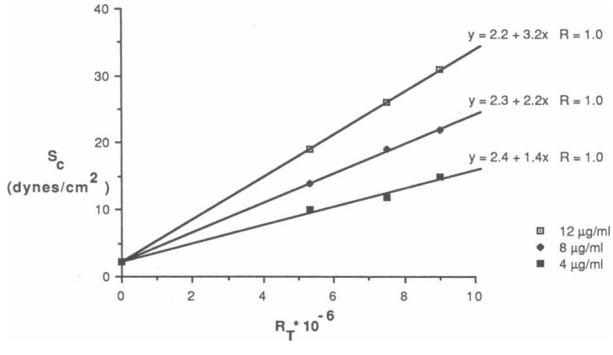

FIGURE 7 Total goat IgG receptor number (R_T) vs. critical shear stress (S_c) for plates coated with either a 4, 8, or 12-μg/ml rabbit anti-goat IgG solution; data are taken from Fig. 6.

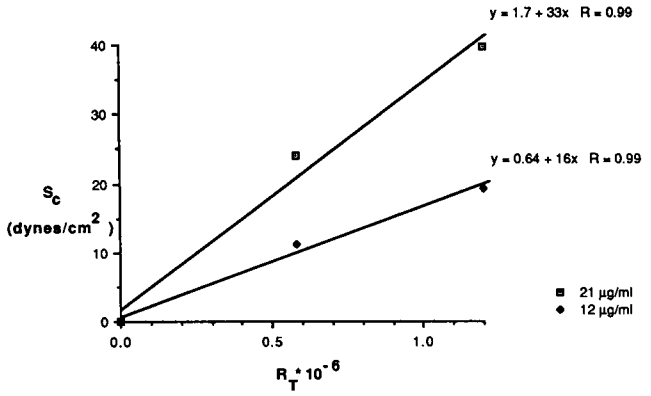

FIGURE 8 Total rabbit anti-goat IgG receptor number (R_T) vs. critical shear stress (S_c) for plates coated with either a 12 or 21-µg/ml solution of goat IgG and three bead types: Cl with ~7.2 × 10^6; and CJ and CL, each with ~3.6 × 10^6 total rabbit anti-goat IgG/bead. The distinction of these data from those in Fig. 7 is goat IgG is coupled to the plate vs. the bead and rabbit anti-goat IgG is coupled to the bead vs. the plate.

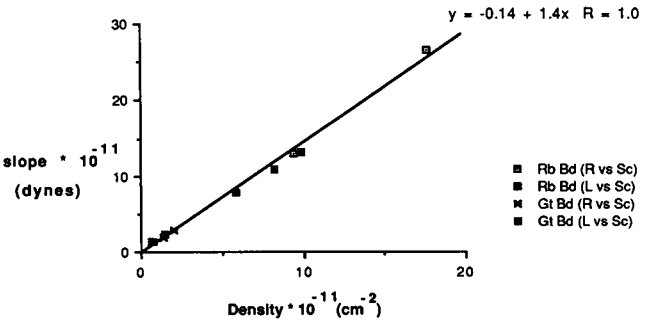

FIGURE 9 The receptor or ligand density vs. the slope of the ligand density vs. critical shear stress (S_c) data or receptor density vs. critical shear stress data, respectively. The conversion from total receptor numbers and ligand coating concentrations to effective receptor and ligand densities, respectively, is explained in Appendix 1. Rb Bd (R vs. Sc) data are from Fig. 8 for rabbit anti-goat IgG coated beads, Rb Bd (L vs. Sc) data are from data taken from Fig. 8 for rabbit anti-goat IgG coated beads, Gt Bd (R vs. Sc) data are from Fig. 7 for goat IgG coated beads, and Gt Bd (L vs. Sc) data are from Fig. 6 for goat IgG coated beads.

The data from Fig. 8 are replotted as L vs. S_c (not shown). The features of these data, which are similar to those in Fig. 6, include a linear increase in S_c with L for a given R_T and an increase in the slope with an increase in R_T. Here, however, the y-intercept is -0.56, consistent with our observation that the nonspecific adhesive force between rabbit anti-goat IgG coated beads and glycine coated plates is small.

By making several assumptions, total receptor numbers and ligand coating concentrations are changed to effective receptor and ligand densities, respectively (Appendix 1). In Fig. 9, the data from Fig. 6 are replotted as goat IgG receptor density vs. the slope of the rabbit anti-goat IgG ligand density vs. S_c data (Gt Bd [L vs. Sc]); the data from Fig. 7 are replotted as rabbit anti-goat IgG ligand density vs. the slope of the goat IgG receptor density vs. S_c data (Gt Bd [R vs. Sc]); the data from Fig. 8 are replotted as goat IgG ligand density vs. the slope of the rabbit anti-goat IgG receptor density vs. S_c data (Rb Bd [R vs. Sc]); and the data for the goat IgG ligand density vs. S_c (not shown but taken from Fig. 8) are replotted as rabbit anti-goat IgG receptor density vs. the slope of the goat IgG ligand density vs. S_c data (Rb Bd [L vs. Sc]). The correlation coefficient for these data is essentially unity. In addition, even if the assumptions made in Appendix 1 were not precisely correct, the slope for these data would still remain constant due to the internal consistency of the model.

Detachment behavior

At the lower range of shear stresses, a percentage of the beads "roll" radially out along the coated surface, attaching and detaching several times before either remaining attached or being swept away. Although this behavior has not been analyzed quantitatively, there are several noticeable trends. First, the shear stress range for this behavior depends on the strength of the interaction between the beads and the surface: the greater the adhesive strength, the higher the values of shear stress supporting this behavior. Second, the actual percentage of beads with this behavior increases then decreases with shear stress; at the highest shear stresses, the beads detach and are swept away from the surface and at the lowest shear stresses, only a small percentage of beads detach. In addition, a bead can serve as a nucleation site for attachment. A bead can detach from a radial position closer to the stagnation point and "roll" to a new radial position next to an adherent bead, where it remains attached.

The critical radius provides a quantitative measure of the adhesive force. In addition, the size of the circular zone of adhesion centered at the stagnation point (see Fig. 2) and the degree of adhesion within this area are indicators of the adhesive strength. The detachment behavior in this region was, however, not analyzed quantitatively because the shear field is not well-characterized. Nevertheless, there were two noticeable detachment trends. First, within a given experiment, the radius of the stagnation zone and the degree of adhesion within this region decreased as the volumetric flow rate increased. Second, at a given volumetric flow rate, the radius of the zone and the degree of adhesion decreased as the value for the critical shear stress decreased, i.e., as the adhesive force decreased.

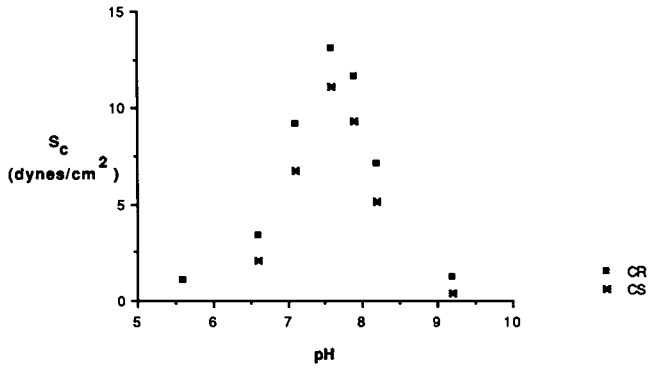

FIGURE 10 The effect of pH on the critical shear stress (S_c) for two bead types, CR and CS, each coated with rabbit anti-goat IgG. The receptor density for CR was ~1.4 times that for CS. The plates were coated with a 12.5-μg/ml solution of goat IgG, and the experiments were run in duplicate or triplicate. The solutions were made up with treated water (pH 7.6, deionized).

Extrinsic properties

pH and ionic strength

The effects of pH and ionic strength on S_c are shown in Figs. 10 and 11, respectively, for plates coated with 12.5-μg/ml goat IgG and two bead types, each coated with rabbit anti-goat IgG. The two bead types used in the pH experiments were CR and CS, where CR had ~1.4 times the receptor density of CS, and the two bead types used in the ionic strength experiments were CT and CU, where CT had approximately twice the receptor density of CU. Figs. 10 and 11 show that treated water (pH 7.6 and ionic strength approximately zero) yields the maximum value for S_c. Each value for S_c is the average for 2–3 experiments. The average value for the percentage error in S_c for the ionic strength and pH experiments is 2 and 5%, respectively (the maximum percentage error is 4 and 6%, respectively). The fact that our pH meter is less accurate (±0.2 pH units) than our scale ($\pm 1 \times 10^{-4}$ g) probably resulted in small fluctuations in pH between the feed solutions, causing larger deviations in the pH than in the NaCl data. The data shown are for the case of the chamber initially filled with the feed used for the given experiment, i.e., the ligand-coated surface was exposed to the feed medium before the bead solution. Several of the ionic strength conditions were rerun for flow cell assembly with the chamber filled with treated water, i.e., the ligand-coated surface was not preexposed to the feed medium. The values for S_c obtained with the two methods agree to within 2%.

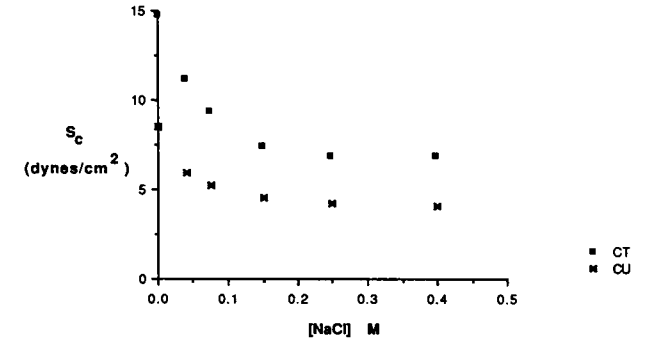

FIGURE 11 The effect of NaCl concentration on the critical shear stress (S_c) for two bead types, CT and CU, each coated with rabbit anti-goat IgG. The receptor density for CT was approximately twice that for CU. The plates were coated with a 12.5-μg/ml solution of goat IgG, and the experiments were run in duplicate or triplicate. The solutions were made up with treated water (pH 7.6, deionized).

DISCUSSION

We have developed a simple cell adhesion assay, the RFDA, to study certain fundamental aspects of receptor-mediated adhesion. The advantages of the RFDA are many, especially direct observation of cell detachment over a range of shear stresses with reproducible, quantitative measurement of the adhesive force. In results reported here, we have studied the interaction between 10 μm diam receptor-coated latex beads (prototype cells) and a ligand-coated glass surface. Rabbit anti-goat IgG and goat IgG were used to simulate the receptor-ligand interaction. The advantages of the coated beads are uniform properties that can be varied in the range typical for cell-to-surface adhesion (Table 1). The shear stress range examined was between 0 and 40 dyn/cm^2, which is within the range of physiological and biotechnological interest. For example, the shear stress in blood vessels is typically between 0 and 100 dyn/cm^2 (0–20 dyn/cm^2 basal and 30–100+ dyn/cm^2 at sharp curvatures and bifurcations [44]); the shear stress in venules and veins, where margination of neutrophils usually occurs, is between 0 and 4 dyn/cm^2 (45); and the shear stress in a typical microcarrier suspension is between 1 and 7 dyn/cm^2 (46).

In this section, we analyze our experimental results with the mathematical model developed for receptor-mediated adhesion in the RFDA. We focus on the effect of the receptor density, ligand density, pH, and ionic strength on the critical shear stress. We also obtain estimates for the number of bonds at a given S_c and for the receptor-ligand (rabbit anti-goat IgG/goat IgG) affinity constant. In addition, we compare the RFDA data and analysis with previous observations on receptor-mediated cell adhesion in other assays (Table 2).

TABLE 2 Experimental results: effect of parameters on adhesive force

Parameter	Value	Adhesive force (cell)	Adhesive force (bead)
Receptor Density (N_R)	Increased	Increase (61)	Linear increase
Ligand Density (N_L)	Increased	Increase (57, 59, 61) Linear increase (60)	Linear increase
pH	Varied	Bell-shaped curve (24, 65*)	Bell-shaped curve
NaCl Concentration	Increased	Decrease (Attractive [67*]) Increase (Repulsive [67*])	Decrease then constant

*Nonspecific adhesion with an attractive or repulsive electrostatic force.

Analysis of parameter effects

The results for the effect of the ligand (rabbit anti-goat IgG) coating concentration (L) on the critical shear stress (S_c) for goat IgG coated beads are shown in Fig. 6. These data indicate that S_c increases linearly with L for a given receptor number per bead (R_T), the slope (the increase in S_c with L) increases as R_T increases, and the y-intercept is not equal to zero. Similar results are obtained for the effect of the ligand (goat IgG) coating concentration on S_c for rabbit anti-goat IgG coated beads (data from Fig. 8). Here, however, the y-intercept is much smaller than that for goat IgG coated beads. The analysis of S_c as a function of N_L predicts that these plots should be linear with a slope of βN_R and a y-intercept of λ, where β is a constant and λ is the critical shear stress in the absence of specific forces (Eq. 8). Therefore, the slope is predicted to increase as R_T (N_R) increases, and λ is predicted to increase as the nonspecific adhesive force increases. The larger value of λ for goat IgG coated beads is, in fact, consistent with the larger nonspecific adhesive force seen between goat IgG coated beads and glycine coated plates.

The results for the effect of the receptor number on S_c for goat IgG coated beads and for rabbit anti-goat IgG coated beads are shown in Figs. 7 and 8, respectively. These data show that S_c increases linearly with R_T for a given L, that the slope increases as L increases, and that the y-intercept corresponds to the value of S_c from the appropriate nonspecific detachment experiment. The analysis of S_c as a function of N_R predicts that these plots have a slope of βN_L and a y-intercept of λ (Eq. 8). Therefore, the slope should increase as L (N_L) increases and the y-intercepts should be consistent with the detachment data for nonspecific adhesion.

By making a number of plausible assumptions, we calculate values for the effective receptor (N_R) and ligand (N_L) densities from the total receptor numbers and ligand coating concentrations, respectively (Appendix 1). In Fig. 9, the slope of each plot for receptor density vs. S_c in Figs. 7 and 8 is plotted as a function of the appropriate ligand density, and the slope of each plot for ligand density vs. S_c in Fig. 6 and from Fig. 8 is plotted as a function of the appropriate receptor density. These data yield a straight line, with a correlation coefficient (R) of unity. From Eq. 8, the data for the slope as a function of N_L and for the slope as a function of N_R are predicted to behave according to the following expressions:

$$S_c/N_R \approx \beta N_L + \lambda/N_R$$

and

$$S_c/N_L \approx \beta N_R + \lambda/N_L,$$

respectively. Therefore, these data are predicted to have a slope of β and a y-intercept of λ/N_R or λ/N_L, respectively. If we assume that the y-intercepts for these data are negligible; the slope is equal to β. Here, $\beta \approx 1.4 \times 10^{-22}$ dyn/cm^2. The fact that β is constant indicates that a given increase in the ligand or receptor density results in a similar increase in S_c, which is consistent with theory (Eq. 7 and 8). Furthermore, regardless of whether the goat IgG is coupled to the bead or plate and the rabbit anti-goat IgG to the plate or bead, respectively, a given increase in either density results in a proportional increase in S_c, demonstrating the symmetry of the system. We must not forget, however, that the number of bonds required for adhesion at a given S_c is actually less for the goat IgG coated beads because λ is larger; therefore, the receptor density required for adhesion at a given S_c is also less for these beads. It is important to realize that even if the assumptions made in Appendix 1 are not precisely correct, the internal consistency of the model will still yield a constant slope for these data. In addition, the specific binding capacity of 0.063 that we estimate for immobilized rabbit anti-goat IgG is in excellent agreement with the measured value of 0.06 obtained by Cress and Ngo (37) for the activity of rabbit anti-human IgG immobilized to a surface via its amine groups. Clearly, the theoretical expression of Eq. 8 is consistent with our data.

We can estimate values for all of the parameters in the expression for β except for $K°$; therefore, we rearrange this expression to solve for $K°$. We assume that $a \approx 0.25$ μm (Appendix 4), $T \approx 296$°K, and $\gamma = 5 \times 10^{-8}$ cm (1), and obtain $K° \approx 1.4 \times 10^{-10}$ cm^2. Perelson et al. (47) derive an expression for the affinity constant (K) of formation of the second bond for singly bound IgG immunoglobulin. In a certain sense, a singly bound IgG antibody is similar to a covalently attached antibody

because there is only one additional bond that can form and the realm of the active site is restricted. Perelson et al. obtain a value of 2.9×10^{-10} cm^2 for K, which is very close to the value that we calculate for the affinity constant of our system. Though less relevant to our system, we also note that experimentally measured values for the affinity constant for hapten-antibody interactions range between 10^{-12}–10^{-2} cm^2 (48). Clearly, our experimental data provide a value for β which yields a reasonable value for the receptor-ligand bond affinity.

Given this value for $K°$, we can use it along with the fixed parameter values from above to determine the total number of bonds (C) required to resist a given S_c (Eq. 6). We assume that $N_L \approx 10^{12}$ cm^{-2}, and obtain the following expression:

$$C \approx 190\, S_c,$$

where S_c is the critical shear stress in dyn/cm^2 (Appendix 3). This expression is applicable to a negligible contribution from the nonspecific forces to the adhesive force. If the net nonspecific force did play a role in countering the hydrodynamic force, C would be approximately equal to the following:

$$C \approx 190\, (S_c - \lambda).$$

In general, the shear stress range studied with the RFDA is between 5 and 30 dyn/cm^2. If we assume that $\lambda \approx 0$, this shear stress range translates into ~1,000–6,000 bonds, respectively, and a bond density (N_b) of between 5×10^{11} and 3×10^{12} cm^{-2}.

The effects of pH and of ionic strength on S_c for rabbit anti-goat IgG coated beads and goat IgG coated plates are shown in Figs. 10 and 11, respectively. Fig. 10 shows that the optimum pH for binding is 7.6 and that S_c decreases sharply as the pH is increased or decreased from this value. Fig. 11 shows that S_c decreases as the NaCl concentration is increased until between 0.15 and 0.25 M, where the value levels off at approximately half that in treated water. For a given N_L and N_R, we predict that a decrease in β and/or λ results in a decrease in S_c (Eq. 8); therefore, these results can be interpreted in terms of the specific and nonspecific interactions.

β is linearly proportional to $K°$; therefore, β provides a measure of the strength of a receptor-ligand bond. In general, the strength of an antibody-antigen bond is the result of the combination of a variety of weak interactions, including electrostatic interactions; therefore, $K°$ is effected by the ionic strength and pH of the liquid medium (49, 50). The general guidelines given by Tijssen (49) and by van Oss and Absolom (50) for antibody-antigen bonds are: electrostatic attraction occurs when the pH is between the isoelectric points of the antigenic determinant and the antibody-active site, electrostatic repulsion can be achieved at low as well as high pH (51, 52), and shielding of the charges with neutral salt ions can dissociate the electrostatic part of the bond (51, 53). It has been shown that the decrease in $K°$ with an increase in ionic strength or a change in pH from the optimum value may result from an increase in the reverse rate constant (51). The trends for the pH and ionic strength data are consistent with those expected for an antibody-antigen interaction. It is, however, important to remember that our proteins are covalently attached to bead and plate surfaces, and these surfaces contribute to the nonspecific component of S_c (λ) and, consequently, may also contribute to these results. The nonspecific adhesive force is also the result of the combination of a variety of weak forces, including electrostatic forces (41). As a result, the nonspecific adhesive force is also effected by the ionic strength and pH of the liquid medium. Therefore, the pH and ionic strength data may, in fact, indicate the effect of these factors on both the nonspecific and specific forces. Finally, note that if we assume that the value for S_c at high salt concentrations levels off because the electrostatic attraction is zero (is completely shielded), then the drop in S_c corresponds to the electrostatic contribution to the adhesive force in treated water.

The pH and ionic data shown are for the flow cell assembled with the feed used for the given experiment, i.e., the ligand-coated surface was exposed to the feed medium before the bead solution. The results obtained when several of the ionic strength conditions were rerun for flow cell assembly with the chamber filled with treated water, i.e., the affinity surface was not exposed to the feed medium before the incubation step, are identical to the results obtained with preexposure (percentage error of 2%). In other words, the critical adhesive force for a given medium is essentially the same regardless of whether the plate is preexposed to that medium. This result can be explained by the fact that the adhesive force is determined after a 30-min exposure to the shear field, which should provide a measure of the equilibrium adhesive force for the given medium. In other words, during the time of shear, the nonspecific and specific interactions are effected by the medium and reach some new equilibrium value. It is obvious that this would be true for the nonspecific interactions; however, it is not unreasonable that this could be true for the antibody-antigen interactions as well. The hydrodynamic force exerted on a bead stresses its bonds with the affinity surface, increasing the value for the reverse rate constant (Eq. 5). In addition, an increase in ionic strength or a change in pH from the optimum value may increase the reverse rate constant. If the adhesive force is greater than or equal to the net fluid force on the bead, a new equilibrium is established. Equilibrium is a dynamic state characterized by essentially a constant number of bonds that continually form

and break. The fact that bond formation is a dynamic process can account for both receptor and ligand exposure to the medium during the time of the experiment.

Comparison with data on cell adhesion

In the experiments reported here, we have examined the detachment of receptor-coated latex beads (prototype cells) from ligand-coated glass surfaces. The beads enable us to examine the effect of various parameters on the adhesive force with particles possessing uniform properties that can be varied systematically. Therefore, we are able to obtain reproducible, quantitative data on adhesion; and avoid the variability that is typical of cells. Our ultimate goal is, however, to obtain data on cell detachment in the RFDA and to analyze these data with a model developed for cell adhesion in the RFDA. We are certainly aware that the interpretation of cell data will be more complicated than that of bead data. For example, on cells, receptors can diffuse into the contact area (54, 55), rather than being fixed to the surface; cells may modulate receptor expression in response to the environment (56), rather than maintaining a fixed receptor number; and cells can settle onto the surface and flatten, increasing the contact area between the cells and surface (13, 57, 58), rather than being resistant to deformation. Nevertheless, cell adhesion data from different assays have shown behavior that is quite similar to that observed for beads in the RFDA (Table 2). Here, we discuss these similarities, while recognizing that rigorous modeling of cell data must include these physiological effects beyond our basic model features.

An increase in the ligand or in the receptor density has been found to increase the adhesive force between cells and surfaces. For example, an increase in the ligand density increases the adhesive force between endothelial cells and fibrinogen-coated coverslips (57) and between the B-cell line MOPC 315 and fibronectin-coated surfaces (59). An approximately linear increase in adhesive force with ligand concentration is seen for the interaction between thymocytes or erythrocytes and lectin-coated fibers (60). For the study on thymocyte adhesion to lectin-coated fibers, the number of bound cells levels off at lectin concentrations greater than $\sim 2 \times 10^{11}$/ml. In addition, an increase in the ligand or in the receptor density increases the adhesive force between various cell types and lectin-coated fibers (61).

Typical values of the affinity constant for cell-related receptor-ligand interactions range between 10^{-11}–10^{-5} cm^2 (62), which encompasses the value calculated for K°. We use the value for K° with the expression developed by Bell (1) for the force of a bond to calculate the number of bonds between a bead and the surface. Capo et al. (28) and Sung et al. (13) use this same expression with their adhesive force data to estimate the number of bonds between thymocytes cross-linked by lectin and between a T-cell and its target cell (TC), respectively. Capo et al. calculate between 1,000 and 3,000 cross-links, and a bond density range of 10^{10}–10^{11} cm^{-2}. Sung et al. estimate 300 bonds and a bond density of 4×10^9 cm^{-2}. In general, estimates for the number of bonds between a T-cell and TC range between 10 and 20,000 with bond densities between 10^7 and 10^{11} cm^{-2} (63). These estimates are based on the contact area and number of receptors per cell. Our estimates for the number of bonds between a bead and a surface are similar to those for a cell and surface. The average bead bond density is feasible because it is within the range of the ligand and receptor densities; however, it is at least an order of magnitude greater than the estimates for the average cell bond density. One possible explanation for higher estimates of the bead bond density is that the radius of the contact area may be larger than the value used in our analysis (0.25 μm). Alternatively, the contact area between a cell and surface may be less than the observed interfacial area because contact may be limited to localized regions (1, 64). In addition, it is possible that a higher bead bond density is, in fact, required because the beads are not deformable. Finally, the equations used to derive this result are based on the assumption that nonspecific forces do not play a role in countering the hydrodynamic force, and this is not necessarily true for our system.

Similar trends for the effect of pH on the adhesive force have been observed for both bacteria and mammalian cells. Fowler (65) studied the effect of pH on the nonspecific adhesive force between bacteria and Pyrex glass or stainless steel. For both interactions, he found that the adhesive force decreases as the pH is either increased or decreased from a value of 7.0. Crouch et al. (24) studied the effect of pH on the adhesion of baby hamster kidney (BHK) cells to glass in the presence of serum, which contained fibronectin, and found that the adhesive force decreases as the pH is increased or decreased from a value of 7.6. In these experiments, it is likely that the fibronectin in the serum adsorbed to the glass, providing specific binding sites for the BHK cells (66).

Gingell and Todd (67) used glutaraldehyde-fixed red blood cells to study the effect of NaCl concentration on the cell-to-glass separation distance for untreated glass surfaces and poly-L-lysine treated glass surfaces. Cells and untreated glass have a net negative charge whereas poly-L-lysine treated glass has a net positive charge. They found that the separation distance between the cells and untreated glass decreases as the salt concentration increases, reaching a minimum in 0.145 M NaCl (physiological saline); however, the separation distance between the

cells and the poly-L-lysine treated surfaces increases with salt concentration, having a minimum value in distilled water. These results indicate that the electrostatic repulsive force between the cells and untreated glass surfaces decreases as the NaCl concentration is increased, and the electrostatic attractive force between the cells and the poly-L-lysine surfaces decreases as the salt concentration is increased. These results are consistent with charge shielding by the salt ions.

The transport behavior observed for bead detachment at the lower range of shear stresses is reminiscent of that seen for neutrophils in blood vessels where they may attach and detach several times before either remaining attached or being swept away (68). This type of behavior can perhaps best be described as saltatory, the result of the cells coming to sudden stops for variable amounts of time. A bead can also serve as a nucleation site for attachment. A bead can detach from a position closer to the stagnation point and "roll" to a position farther out and next to another bead, where it can reattach. Particle aggregation has also been observed in attachment assays with neutrophils (17, 69).

Finally, the detachment behavior seen in the zone centered at the stagnation point is similar to that observed for leukocytes by Nyilas et al. (70). These investigators used flowing blood as the source to an axisymmetric flow assay and examined adhesion exclusively at the stagnation region. They saw a circular zone of leukocyte adhesion, the radius of which decreased on a given surface as the flow rate increased and decreased at a given flow rate as the adhesive strength (thrombogenicity of the surface) decreased.

APPENDIX 1

Description of IgG and analysis of effective coating concentration

The two-dimensional structure of an IgG immunoglobulin molecule is shown in Fig. A1. The molecule is composed of two identical light chains and two identical heavy chains linked together by disulfide bonds (71). The part of the molecule that includes the disulfide bonds between the heavy chains is referred to as the hinge region. Studies on IgG suggest that there is considerable flexibility in this region, allowing rotation of the heavy/light chain "arms" as well as variation in the distance between the two identical antigen binding sites (72). The tail of the antibody, where the heavy chains are paired, is called the Fc region. The affinity constant of an antibody-antigen reaction is a measure of the strength of the interaction between the antibody active site and the antigenic determinant. The term avidity is used to describe the net strength of the interaction between the antibody and a multideterminant antigen, i.e., the strength when both active sites can bind to determinants on the same antigen. In general, the IgG avidity is $\sim 10^2$–10^4 times the affinity (47, 73).

When IgG from one animal (for example, goat) is injected into a suitable second animal (for example, rabbit), the injected antibody causes the production of host antibodies (rabbit anti-goat IgG antibodies). The host antibodies are directed against different sites (determinants or epitopes) on the injected antibody; therefore, they are called polyclonal antibodies. In general, the antibodies directed against a given epitope are identical. The total number of epitopes (n_E) on a given antigen can be estimated with the following expression (50):

$$n_E = (M_w/5{,}000)^{2/3},$$

where M_w is the molecular weight of the antigen. For goat IgG, $M_w \approx$ 160,000; therefore, $n_E \approx 10$.

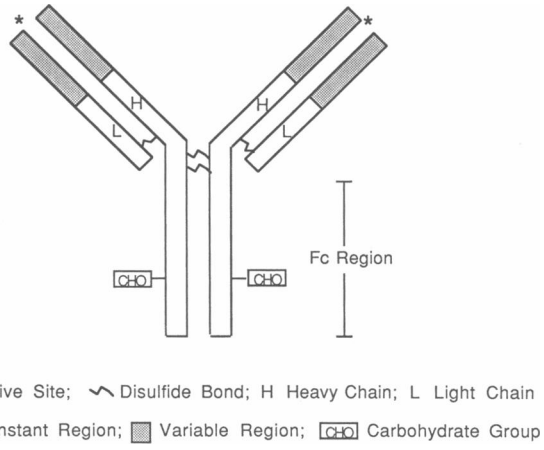

FIGURE A1 Schematic diagram of an IgG immunoglobulin molecule.

In our experiments, ligand and receptors are covalently coupled to the surface of a plate and beads, respectively. Specific binding between a cell and a surface requires alignment of the receptor binding site with the ligand site. This involves translational and orientational diffusion of the receptor to a proper position and orientation required for reaction (74). Rutishauser and Sachs found glutaraldehyde fixed cells are unable to bind to either lectin-coated fibers (61) or lectin-treated glutaraldehyde fixed cells (75, 76). They attribute this effect to the loss of both long and short-range movement of the receptors. Specific binding can occur between our model cells and surfaces because the size and structure, in particular the hinge region, of the IgG immunoglobulins enable orientation of receptor binding sites with antigenic determinants.

Ligand is covalently coupled to the surface with glutaraldehyde and receptor with carbodiimide (Materials and Methods). Both techniques couple the protein via its amine groups, resulting in a loss in protein activity (see Fig. A2) (36). A general guideline for antibody is no more than one antibody-active site available and 20–50% of those sites active (35). To estimate the effective concentration of receptor and ligand on the surfaces, both the loss in activity caused by the coupling procedure and the polyclonal nature of the antibody have to be considered. We assume no more than one binding site per rabbit anti-goat IgG, and a

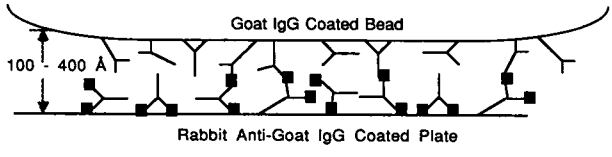

FIGURE A2 Schematic diagram of interacting receptors and ligands, both of which are covalently coupled to the surface via amine groups.

35% activity. If there were a way to distinguish one binding site of an IgG molecule from the other, 50% of the active sites would probably be of one type and 50% of the other; therefore, the probability that a given site would be active (P_A) would be $0.35/2 \approx 0.18$. We assume that the total probability of active sites for rabbit anti-goat IgG ($P_{A[Rb]}$) is equal to the number of binding sites per molecule times P_A:

$$P_{A(Rb)} = (2 \text{ sites/Rb}) * (0.18/\text{site}) = 0.36.$$

A similar analysis is used to determine the total probability of active determinants for goat IgG ($P_{A[Gt]}$):

$$P_{A(Gt)} = (10 \text{ epitopes/Gt}) * (0.18/\text{site}) = 1.8.$$

To determine the probability that the antibody is complementary to the epitope and vice versa, a couple of simplifying assumptions are made. First, steric hindrance is negligible, i.e., if the antibody and antigen are active, complementary, and within reach of each other, they will be able to bind. Second, the number of epitopes is much greater than the number of antibody binding sites, i.e., there is a goat IgG molecule across from each antibody binding site. Therefore, the probability that the antibody is complementary ($P_{S[Rb]}$) is equal to the number of active epitopes available to the antibody divided by the total number of subclasses of antibody directed against the antigen, which is, in general, equal to the total number of epitopes:

$$P_{S(Rb)} = (1.8 \text{ epitopes/Gt}) * (\text{Gt}/10 \text{ epitopes}) = 0.18.$$

The probability that the epitope is complementary ($P_{S[Gt]}$) is equal to the number of active epitopes divided by the total number of epitopes:

$$P_{S(Gt)} = (1.8 \text{ epitopes/Gt}) * (\text{Gt}/10 \text{ epitopes}) = 0.18.$$

The final result for the effective concentration of rabbit anti-goat IgG (N_{Rb}) and of goat IgG (N_{Gt}) is:

$$N_{Rb} = N_{T(Rb)} * P_{A(Rb)} * P_{S(Rb)} = 0.063\, N_{T(Rb)}$$

and

$$N_{Gt} = N_{T(Gt)} * P_{A(Gt)} * P_{S(Gt)} = 0.32\, N_{T(Gt)},$$

respectively, where $N_{T(Rb)}$ and $N_{T(Gt)}$ are the total rabbit anti-goat IgG and the total goat IgG surface densities (cm^{-2}), respectively. Cress and Ngo (37) measured the specific binding capacity of rabbit anti-human IgG immobilized to a surface via its amine groups and obtained a value of 0.06 mg human IgG per milligram rabbit IgG, in excellent agreement with our predictions.

The total surface concentrations for beads are determined analytically; however, this technique cannot be used to determine the surface concentrations for plates because the concentrations are too low (Materials and Methods). As a result, the total surface density for plates is estimated by making a couple of assumptions. First, the surface "sees" ~2 ml of the coating solution (the plates are submerged in a Petri dish [approximate diameter of 52 mm] with 5 ml of the coating solution, and, in general, the height of fluid above the coated surface [upper surface] was 1 mm). Second, 70% of the protein is coupled to the plate (35). The total surface density ($N_{T[L]}$) is calculated from:

$$N_{T(L)} = 0.7 \text{ L} * (2 \text{ ml}) * \{A_v/[\pi\rho_G^2(M_w)]\},$$

where L is the concentration of the ligand coating solution (μg/ml), A_v is Avogadro's number, ρ_G is the radius of the glass disc (25 mm), and M_w is the molecular weight of IgG (160,000).

The site-specific coupling of IgG through the carbohydrate groups located on the Fc region (Fig. A1), as opposed to random coupling through amine groups has been found to result in a 30–400% increase in the IgG antigen binding capacity (increase in $P_{A[Ab]}$) (77). This increase is attributed to the fact that the active sites are spacially discrete from the Fc region. This coupling method is ideally suited for processes such as affinity chromatography (37, 77); however, it was not chosen for our experiments to avoid the potential problems caused by avidity. For example, if only a percentage of the antibodies could form two bonds, large variations in bond strength would occur. Further, if the net adhesive force were too strong, turbulent flow would be required to detach the beads.

APPENDIX 2

Calculation of bead separation distance

The mean distance between receptors on a cell (b) can be estimated as:

$$b \approx [(s_A)/R_T]^{1/2},$$

where s_A is the surface area of the cell and R_T is the number of receptors per cell. We adapt this expression to obtain an estimate for the number of beads required for a given separation distance on the affinity surface:

$$n_B = \pi\rho_P^2/d^2,$$

where n_B is the total number of beads on the affinity surface at the start of a given experiment, ρ_P is the flow cell radius for axisymmetric flow (the radius of the Plexiglass cylinder [12.7 mm]), and d is the average distance from the center of one bead to the center of the next. The bead concentration (c) required for a given d is determined by dividing n_B by the volume for axisymmetric flow:

$$c = n_B/(\pi\rho_P^2 h),$$

where h is the gap width (0.254 mm). For example, if d were to be seven bead diameters, ~70 μm, then c and n_B would need to be 8×10^5 beads/ml and 1×10^5, respectively.

APPENDIX 3

Detailed derivation of mathematical model

For a particle to remain attached to a surface, the adhesive force must balance the force and torque imposed by the passing fluid. The force (F_s) and torque (T) on an adherent particle at the critical radius are estimated with the following expressions of Goldman et al. (39) for the force and torque on a stationary sphere in a shear field:

$$F_s = 6\pi S_c(\rho_B + h_s)\rho_B F_s^* \qquad \text{(A1)}$$

and

$$T = 4\pi S_c(\rho_B)^3 T^*, \qquad \text{(A2)}$$

respectively, where S_c is the critical shear stress (Eq. 2), ρ_B is the bead radius, h_s is the separation distance between the bead and plate (Fig. A3), and F_s^* and T^* are functions of the ratio $(\rho_B + h_s)/\rho_B$. The dimensions of an IgG molecule are ~240 × 57 × 19 Å (35). Hence, the maximum value for h_s is ~2 × 240 Å (0.048 μm), resulting in a maximum value for $(\rho_B + h_s)/\rho_B$ of 1.01. For $(\rho_B + h_s)/\rho_B$ between

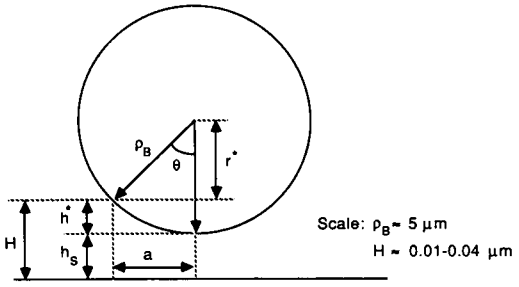

FIGURE A3 Illustration of a bead in contact with the surface, where h_s is the separation distance between the bead and plate, H is the maximum separation distance for receptor-ligand binding, and ρ_B and a are the radius of the bead and contact area, respectively.

1.00 and 1.01, reasonable values for F_s^* and T* are 1.7 and 0.94, respectively (39).

The total force exerted on an adherent particle is estimated with the force and torque balance developed by Hammer and Lauffenburger (2) for receptor-mediated adhesion. Their model is based on the following assumptions: the adhesive force acts both parallel to the direction of flow and normal to the particle surface, the nonspecific forces do not contribute to the net adhesive force, and the bond densities and force per bond are constant over the contact area. Their result for the total force exerted on an adherent particle is:

$$F_T = \{F_s^2 + (9\pi^2/16a^2)[T^2 + 2TF_s\rho_B + (F_s\rho_B)^2]\}^{1/2}, \quad \text{(A3)}$$

where a is the radius of the contact area (Fig. A3). We assume $\rho_B \approx \rho_B + h_s$, and obtain the following result for the total force exerted on an adherent particle at the critical radius:

$$F_T \approx S_c\rho_B^2[(1.0 \times 10^3) + (1.1 \times 10^4)(\rho_B/a)^2]^{1/2}. \quad \text{(A4)}$$

Because a is limited to a maximum value of ~0.5 μm (Appendix 4) and $1.0 \times 10^3 \ll 1.1 \times 10^4\,(5/0.5)^2 = 1.1 \times 10^6$, we assume:

$$F_T \approx 110S_c\rho_B^3/a. \quad \text{(A5)}$$

The force of a bond (F_b) is estimated with the following expression developed by Bell (1):

$$F_b \approx (0.7k_bT/\gamma) \ln (K^oN_L), \quad \text{(A6)}$$

where k_b is the Boltzman constant, T is the temperature, γ is the range of the interaction (~5×10^{-8} cm for an antigen-antibody bond [1]), N_L is the ligand density, and K^o is the receptor-ligand affinity constant (k_f^o/k_r^o). If we assume that the contribution from the nonspecific forces to the adhesive force is negligible and the bonds are equally distributed and stressed, then:

$$F_T = F_bC, \quad \text{(A7)}$$

where C is the total number of receptor-ligand complexes (bonds). Using the expressions for F_T (Eq. A5) and F_b (Eq. A6) in Eq. A7, we obtain the following expression for the total number of bonds required for adhesion at the critical radius:

$$C = (160\gamma/k_bT)[S_c/\ln (K^oN_L)](\rho_B^3/a). \quad \text{(A8)}$$

Eq. A8 predicts that the number of bonds is directly proportional to the critical shear stress. Hammer and Lauffenburger (2) develop the following expression for the total receptor density required for receptor-mediated adhesion under equilibrium conditions:

$$N_R = (\gamma F_T/k_bT)(e/\pi a^2K^oN_L), \quad \text{(A9)}$$

where N_R is the receptor density. The expression for the total receptor density required for adhesion at the critical radius is obtained by using the result for F_T (Eq. A5) in Eq. A9:

$$N_R \approx 33e[S_c/(K^oN_L)](\gamma/k_bT)(\rho_B/a)^3. \quad \text{(A10)}$$

This equation is rearranged to the following:

$$S_c \approx \beta N_LN_R, \quad \text{(A11)}$$

where:

$$\beta = (K^o/33e)(k_bT/\gamma)(a/\rho_B)^3.$$

APPENDIX 4

Calculation of contact area

A schematic diagram of a bead in contact with a surface is shown in Fig. A3, which is not drawn to scale. The important parameters are: ρ_B, the radius of the particle (known); h_s, the separation distance between the bead and plate, and H, the maximum separation distance for receptor-ligand binding (varied in the model); and a, the radius of the contact area (calculated with the model). The relationship between h_s, H, and a is derived for this geometry. We define, as shown in Fig. A3:

$$h^* = H - h_s$$

and

$$r^* = \rho_B - h^*$$

θ and a are given by:

$$\theta = \cos^{-1}(r^*/\rho_B)$$

and

$$a = \rho_B \sin \theta,$$

respectively. The dimensions of IgG are ~19 × 57 × 240 Å (35); therefore, h_s and H are limited to values between ~100 and 400 Å, with $H \geq h_s$. From this model, we conclude that a is equal to 0 when H is equal to h_s, the contact area radius (a) increases as H increases and/or h_s decreases, and the maximum value for a (H = 400 Å and h_s = 100 Å) is 0.5 μm.

This model is similar to that developed by Hubbe (78) to calculate the characteristic radius of the contact area between a colloidal particle and a surface, where H is the characteristic height of the surface roughness of the particle. In our analysis, we assume that the characteristic height of the surface roughness is negligible with respect to the maximum length for bond formation. If this were not the case, the analysis could be adjusted to account for both effects; however, the final result would probably be close to the same because the loss in contact area from indentations would be gained by protrusions.

The authors wish to thank Daniel A. Hammer for several helpful conversations and Joseph Yanez for preparation of the standard curve for absorbance vs. bead concentration.

This work was supported by National Science Foundation grant EET 87-12784 from the Biotechnology Program. Financial support from an AAUW Selected Professions Fellowship to C. Cozens-Roberts is also gratefully acknowledged.

Received for publication 20 June 1989 and in final form 27 November 1989.

REFERENCES

1. Bell, G. I. 1978. Models for the specific adhesion of cells to cells. *Science (Wash. DC)*. 200:618–627.
2. Hammer, D. A., and D. A. Lauffenburger. 1987. A dynamic model for receptor-mediated cell adhesion to surfaces. *Biophys. J.* 52:475–487.
3. Thomas, P. D., F. W. Hampson, and G. W. Hunninghake. 1988. Neutrophil adherence to human endothelial cells. *J. Lab. Clin. Med.* 111:286–292.
4. Chin, Y.-H., R. Rasmussen, A. G. Cakiroglu, and J. J. Woodruff. 1984. Lymphocyte recognition of lymph node high endothelium. VI. Evidence of distinct structures mediating binding to high endothelial cells of lymph nodes and Peyer's patches. *J. Immunol.* 133:2961–2965.
5. Butcher, E. C., R. G. Scollay, and I. L. Weissman. 1980. Organ specificity of lymphocyte migration: mediation by highly selective lymphocyte interaction with organ-specific determinants on high endothelial venules. *Eur. J. Immunol.* 10:556–561.
6. Jauregui, H. O. 1987. Cell adhesion to biomaterials: the role of several extracellular matrix components in the attachment of non-transformed fibroblasts and parenchymal cells. *Trans. Am. Soc. Artif. Intern. Organs.* 33:66–74.
7. Anderson, J. M. 1988. Inflammatory response to implants. *Trans. Am. Soc. Artif. Intern. Organs.* 34:101–107.
8. Seeger, R. C., D. D. Vo, J. Ugelstad, and C. P. Reynolds. 1986. Removal of neuroblastoma cells from bone marrow with monoclonal antibodies and magnetic immunobeads. *In* Transfusion Medicine: Recent Technological Advances. K. Murawski and F. Peetoom, editors. Alan R. Liss, Inc., New York. 285–293.
9. Berenson, R. J., L. J. Levitt, R. Levy, and R. A. Miller. 1984. Cellular immunosorption using monoclonal antibodies. *Transplantation (Baltimore)*. 38:136–143.
10. Hubbe, M. A. 1981. Adhesion and detachment of biological cells in vitro. *Prog. Surf. Sci.* 11:65–138.
11. Evans, E. A. 1980. Minimum energy analysis of membrane deformation applied to pipet aspiration and surface adhesion of red blood cells. *Biophys. J.* 30:265–284.
12. Evans, E., and A. Leung. 1984. Adhesivity and rigidity of erythrocyte membrane in relation to wheat germ agglutinin binding. *J. Cell Biol.* 98:1201–1208.
13. Sung, K. P., L. A. Sung, M. Crimmins, S. J. Burakoff, and S. Chien. 1986. Determination of junction avidity of cytolytic T cell and target cell. *Science (Wash. DC)*. 234:1405–1408.
14. Easty, G. C., D. M. Easty, and E. J. Ambrose. 1960. Studies of cellular adhesiveness. *Exp. Cell Res.* 19:539–548.
15. McClay, D. R., G. M. Wessel, and R. B. Marchase. 1981. Intercellular recognition: quantitation of initial binding events. *Proc. Natl. Acad. Sci. USA.* 78:4975–4979.
16. Doroszewski, J. 1980. Short-term and incomplete cell-substrate adhesion. *In* Cell Adhesion and Motility. A. S. G. Curtis and J. D. Pitts, editors. Cambridge University Press, New York. 171–197.
17. Forrester, J. V., and J. M. Lackie. 1984. Adhesion of neutrophil leukocytes under conditions of flow. *J. Cell Sci.* 70:93–110.
18. Barabino, G. A., L. V. McIntire, S. G. Eskin, D. A. Sears, and M. Udden. 1987. Endothelial cell interactions with sickle cell, sickle trait, mechanically injured, and normal erythrocytes under controlled flow. *Blood.* 70:152–157.
19. Weiss, L. 1961. The measurement of cell adhesion. *Exp. Cell Res.* 8:141–153.
20. Pratt, K. J., B. E. Jarrell, S. K. Williams, R. A. Carabasi, M. A. Rupnick, and M. A. Hubbard. 1988. Kinetics of endothelial cell-surface attachment forces. *J. Vasc. Surg.* 7:591–599.
21. Worthen, G. S., L. A. Smedly, M. G. Tonnesen, D. Ellis, N. F. Voelkel, J. T. Reeves, and P. M. Henson. 1987. Effects of shear stress on adhesive interaction between neutrophils and cultured endothelial cells. *J. Appl. Physiol.* 63:2031–2041.
22. Fowler, H. W., and A. J. McKay. 1980. The measurement of microbial adhesion. *In* Microbial Adhesion to Surfaces. R. C. W. Berkeley, J. M. Lynch, J. Melling, P. R. Rutter, and B. Vincent, editors. Ellis Horwood Limited, Chichester, England. 143–161.
23. Duddridge, J. E., C. A. Kent, and J. F. Laws. 1982. Effect of surface shear stress on the attachment of *Pseudomonas fluorescens* to stainless steel under defined flow conditions. *Biotechnol. Bioeng.* 24:153–164.
24. Crouch, C. J., H. W. Fowler, and R. E. Spier. 1985. The adhesion of animal cells to surfaces: the measurement of critical surface shear stress permitting attachment or causing detachment. *J. Chem. Technol. Biotechnol.* 35B:273–281.
25. Groves, B. J., and P. A. Riley. 1987. A miniaturised parallel-plate shearing apparatus for the measurement of cell adhesion. *Cytobios.* 52:49–62.
26. Cozens-Roberts, C., D. A. Lauffenburger, and J. A. Quinn. Receptor-mediated cell attachment and detachment kinetics: part I—probabilistic model and analysis. *Biophys. J.* In press.
27. Cozens-Roberts, C., J. A. Quinn, and D. A. Lauffenburger. Receptor-mediated cell attachment and detachment kinetics: part II—experimental model studies with the radial-flow detachment assay. *Biophys. J.* In press.
28. Capo, C., F. Garrouste, A. Benoliel, P. Bongrand, A. Ryter, and G. I. Bell. 1982. Concanavalin-A-mediated thymocyte agglutination: a model for a quantitative study of cell adhesion. *J. Cell Sci.* 56:21–48.
29. Bongrand, P., C. Capo, A. M. Benoliel, and R. Depieds. 1979. Evaluation of intercellular adhesion with a very simple technique. *J. Immunol. Methods.* 28:133–141.
30. Pelton, R. H., and L. H. Allen. 1984. Factors influencing the adhesion of polystyrene spheres attached to pyrex by polyethyleneimine in aqueous solution. *J. Colloid Interface Sci.* 99:387–398.
31. Mege, J. L., C. Capo, A. M. Benoliel, and P. Bongrand. 1986. Determination of binding strength and kinetics of binding initiation: a model study made on the adhesive properties of P388D1 macrophage-like cells. *Cell. Biophys.* 8:141–160.
32. Weetal, H. H. 1976. Covalent coupling methods for inorganic support materials. *Methods Enzymol.* 44:134–148.
33. von Tscharner, V., and H. M. McConnell. 1981. Physical properties of lipid monolayers on alkylated planer glass surfaces. *Biophys. J.* 36:421–427.

34. Molday, R. S., W. J. Dreyer, A. Rembaum, and S. P. S. Yen. 1975. New immunolatex spheres: visual makers of antigens on lymphocytes for scanning electron microscopy. *J. Cell Biol.* 64:75–88.

35. Clausen, J. 1981. Immunochemical techniques for the identification and estimation of macromolecules. *In* Laboratory Techniques in Biochemistry and Molecular Biology. Vol. 1 (3). T. S. Work and E. Work, editors. North-Holland Publishing Co., New York. 387 pp.

36. Galloway, R. J. 1988. Development of Microparticle Tests and Immunoassays. Seradyn, Inc., Indianapolis, IN. 38 pp.

37. Cress, M. C., and T. T. Ngo. 1989. Site specific immobilization of immunoglobulins. *Am. Biotechnol. Lab.* 7:16–19.

38. Moller, P. S. 1963. Radial flow without swirl between parallel discs. *Aeronautical Quarterly.* 14:163–186.

39. Goldman, A. J., R. G. Cox, and H. Brenner. 1967. Slow viscous motion of a sphere parallel to a plane wall-II Couette flow. *Chem. Eng. Sci.* 22:653–660.

40. Zhurkov, S. N. 1965. Kinetic concept of the strength of solids. *Int. J. Frac. Mech.* 1:311–323.

41. Bongrand, P., and G. I. Bell. 1984. Cell-cell adhesion: parameters and possible mechanisms. *In* Cell Surface Dynamics: Concepts and Models. A. S. Perelson, C. DeLisi, and F. W. Wiegel, editors. Marcel Dekker, Inc., New York. 459–493.

42. Pinckard, R. N. 1973. Equilibrium dialysis and preparation of hapten conjugates. *In* Handbook of Experimental Immunology. D. M. Weir, editor. Blackwell Scientific Publications, London. 17.1–17.22.

43. Werblin, T. P., and G. R. Siskind. 1972. Distribution of antibody affinities: technique of measurement. *Immunochemistry.* 9:987–1011.

44. Dewey, C. F. 1979. Fluid mechanics of arterial flow. *In* Dynamics of Arterial Flow. S. Wolf and N. T. Werthessen, editors. *Adv. Exp. Med. Biol.* 115:55–103.

45. Lawrence, M. B., L. V. McIntire, and S. G. Eskin. 1987. Effect of flow on polymorphonuclear leukocyte/endothelial cell adhesion. *Blood.* 5:1284–1290.

46. Cherry, R. S., and E. T. Papoutsakis. 1986. Hydrodynamic effects on cells in agitated tissue culture reactors. *Bioprocess Eng.* 1:29–41.

47. Perelson, A. J., B. Goldstein, and S. Rocklin. 1980. Optimal strategies in immunology III. The IgM-IgG switch. *J. Math. Biol.* 10:209–256.

48. Pecht, I., and D. Lancet. 1977. Kinetics of antibody-hapten interactions. *Mol. Biol. Biochem. Biophys.* 24:306–338.

49. Tijssen, P. 1985. Practice and theory of immunoassays. *In* Laboratory Techniques in Biochemistry and Molecular Biology. Vol. 15. R. H. Burden and P. H. van Knippenberg, editors. Elsevier, New York. 549 pp.

50. van Oss, C. J., and D. R. Absolom. 1984. Nature and thermodynamics of antigen-antibody interactions. *In* Molecular Immunology. M. Z. Atassi, C. J. van Oss, and D. R. Absolom, editors. Marcel Dekker, Inc., New York. 337–360.

51. Hughes-Jones, N. C., B. Gardner, and R. Telford. 1964. The effect of pH and ionic strength on the reaction between anti-D and erythrocytes. *Immunology.* 7:72–81.

52. van Oss, C. J., D. R. Absolom, A. L. Grossberg, and A. W. Neumann. 1979. Repulsive van der Waals forces. 1. Complete dissociation of antigen-antibody complexes by means of negative van der Waals forces. *Immunol. Commun.* 8:11–29.

53. deGroot, E. R., M. C. Lamers, L. A. Aarden, R. J. T. Smeenk, and C. J. van Oss. 1980. Dissociation of DNA/anti-DNA complexes at high pH. *Immunol. Commun.* 9:515–528.

54. Hafeman, D. G., von Tscharner, V., and H. M. McConnell. 1981. Specific antibody-dependent interactions between macrophages and lipid haptens in planar lipid monolayers. *Proc. Natl. Acad. Sci. USA.* 78:4552–4556.

55. Wilkinson, P. C., J. M. Lackie, J. V. Forrester, and G. A. Dunn. 1984. Chemokinetic accumulation of human neutrophils on immune complex-coated substrata: analysis at a boundary. *J. Cell. Biol.* 99:1761–1768.

56. Estrabrook, A., C. L. Berger, R. Mittler, P. LoGerfo, M. Hardy, and R. L. Edelson. 1983. Antigenic modulation of human T-lymphocytes by monoclonal antibodies. *Transplant. Proc.* 15: 651–656.

57. Dejana, E., S. Colella, L. R. Languino, G. Balconi, G. C. Corbascio, and P. C. Marchisio. 1987. Fibrinogen induces adhesion, spreading, and microfilament organization of human endothelial cells in vitro. *J. Cell Biol.* 104:1403–1411.

58. Eskin, S. G., C. L. Ives, L. V. McIntire, and L. T. Navarro. 1984. Response of cultured endothelial cells to steady flow. *Microvasc. Res.* 28:87–94.

59. Liao, N., J. St. John, Z. J. Du, and H. T. Cheung. 1987. Adhesion of lymphoid cell lines to fibronectin-coated substratum: biochemical and physiological characterization and the identification of a 140-kDa fibronectin receptor. *Exp. Cell Res.* 171:306–320.

60. Edelman, G. M., U. Rutishauser, and C. F. Millette. 1971. Cell fractionation and arrangement on fibers, beads, and surfaces. *Proc. Natl. Acad. Sci. USA.* 68:2153–2157.

61. Rutishauser, U., and L. Sachs. 1975. Receptor mobility and the binding of cells to lectin-coated fibers. *J. Cell Biol.* 66:76–85.

62. Bell, G. I., M. Dembo, and P. Bongrand. 1984. Cell adhesion: competition between nonspecific repulsion and specific bonding. *Biophys. J.* 45:1051–1064.

63. Berke, G. 1983. Cytotoxic T-lymphocytes: how do they function? *Immuno. Rev.* 72:5–42.

64. Burridge, K., K. Fath, T. Kelly, G. Nuckolls, and C. Turner. 1988. Focal adhesions: transmembrane junctions between the extracellular matrix and the cytoskeleton. *Annu. Rev. Cell. Biol.* 4:487–525.

65. Fowler, H. W. 1988. Microbial adhesion to surfaces. *In* CRC Handbook of Laboratory Model Systems for Microbial Ecosystems. J. W. T. Wimpenny, editor. CRC Press, Inc., Boca Raton, FL. 139–153.

66. Hughes, R. C., S. D. J. Pena, J. Clark, and R. R. Dourmashkin. 1979. Molecular requirements for the adhesion and spreading of hamster fibroblasts. *Exp. Cell Res.* 121:307–314.

67. Gingell, D., and I. Todd. 1980. Red blood cell adhesion—II. Interferometric examination of the interaction with hydrocarbon oil and glass. *J. Cell Sci.* 41:135–149.

68. Atherton, A., and G. V. R. Born. 1972. Quantitative investigations of the adhesiveness of circulating polymorphonuclear leukocytes to blood vessel walls. *J. Physiol.* 222:447–474.

69. McIntire, L. V., and S. G. Eskin. 1984. Mechanical and biochemical aspects of leukocyte interactions with model vessel walls. *In* White Cell Mechanics: Basic Science and Clinical Aspects. H. J. Meiselman, M. A. Lichtman, and P. L. LaCelle, editors. Alan R. Liss, Inc., New York. 209–219.

70. Nyilas, E., W. A. Morton, D. M. Lederman, T.-H. Chiu, and R. D. Cumming. 1975. Interdependence of hemodynamic and surface parameters in thrombosis. *Trans. Amer. Soc. Artif. Organs.* 21:55–64.

71. Hood, L. E., I. L. Weissman, W. B. Wood, and J. H. Wilson. 1984. Immunology. The Benjamin/Cummings Publishing Co., Inc., Menlo Park, CA. 558 pp.

72. Crothers, D. M., and H. Metzger. 1972. The influence of polyvalency on the binding properties of antibodies. *Immunochemistry*. 9:341–357.

73. Alberts, B., D. Bray, J. Lewis, M. Raff, K. Roberts, and J. D. Williams. 1983. Molecular Biology of the Cell. Garland Publishing, Inc., New York. 1146 pp.

74. Lauffenburger, D., and C. DeLisi. 1983. Cell surface receptors: physical chemistry and cellular regulation. *Int. Rev. Cytol.* 84:269–302.

75. Rutishauser, U., and L. Sachs. 1974. Receptor mobility and the mechanism of cell-cell binding induced by concanavalin A. *Proc. Natl. Acad. Sci. USA*. 71:2456–2460.

76. Rutishauser, U., and L. Sachs. 1975. Cell-to-cell binding induced by different lectins. *J. Cell Biol.* 65:247–257.

77. Little, M. C., C. J. Siebert, and R. S. Marson. 1988. Enhanced antigen binding to IgG molecules immobilized to a chromatographic support via their Fc domains. *Biochromatography*. 3:156–160.

78. Hubbe, M. A. 1984. Theory of detachment of colloidal particles from flat surfaces exposed to flow. *Colloids Surf.* 12:151–178.

79. Schmid-Schoenbein, G. W., Y. Fung, and B. W. Zweifach. 1975. Vascular endothelium-leukocyte interactions: sticking shear force in venules. *Circ. Res.* 36:173–184.